Nonlinear Optical Properties and Crystalline Orientation of 2-Methyl-4-nitroaniline Layers Grown on Nanostructured Poly(tetrafluoroethylene) Substrates

R. Vallée,[†] P. Damman,*[,†] M. Dosière,[†] E. Toussaere,[‡] and J. Zyss[‡]

Contribution from the Laboratoire de Physicochimie des Polymères, Université de Mons-Hainaut, 20, Place du Parc, B-7000 Mons, Belgique, and Ecole Normale Supérieure de Cachan, Laboratoire de Photonique Quantique et Moléculaire (UMR CNRS No. 8537) 61, Avenue Président Wilson, 94235 Cachan Cedex, France

Received June 7, 1999. Revised Manuscript Received April 20, 2000

Abstract: A new methodology to study the second-order nonlinear optical coefficients of organic materials was developed. The combination of oriented crystal growth (epitaxy or grapho-epitaxy) with grazing incidence X-ray diffraction and second harmonic ellipsometry gives an overview of the relations between the molecular hyperpolarizability and the crystalline nonlinear susceptibility tensor. Thin organic layers of 2-methyl-4-nitroaniline (MNA) were grown on nanostructured poly(tetrafluoroethylene) (PTFE) substrates prepared by the friction transfer method. The investigations show that MNA crystallizes with two definite single-crystal-like orientations depending on the substrate temperature. The low- and high-temperature modes of growth correspond to a deposit of the aromatic ring more or less flat ((11−2) orientation) or edge ((010) orientation) on the substrate, respectively, the transition temperature corresponding to the first order−disorder transition of PTFE (∼19 °C). Two different orientation mechanisms were then proposed. At low temperature, the intermolecular interactions at the overlayer−substrate interface induce a coincident epitaxy that corresponds to a specific physisorption of aromatic molecules on the polymer surface, whereas above the PTFE order−disorder phase transition, the drastic decrease of the nucleation rate strongly suggests that the orientation is achieved via a grapho-epitaxy that occurs on topological defects of the surface. From the second harmonic ellipsometry measurements, the ratio between the nonvanishing components of the first nonlinear susceptibility tensor (χ_{ijk} or d_{ij}) was measured. Finally, the experimental observations were discussed in relation to the oriented gas model and the components of the molecular hyperpolarizability tensor (β_{ijk}).

Introduction

As previously demonstrated by several authors, highly oriented nanostructured poly(tetrafluoroethylene) (PTFE) films can be obtained by sliding a PTFE rod on glass slides.[1−3] These films, a few tens of a nanometer thick, exhibit a single-crystal orientation and can be used to induce the growth of different organic or macromolecular crystals.[1,4−8] However, despite the large number of papers devoted to this subject, the mechanism by which these PTFE films induce the orientation is not fully understood.

These PTFE substrates somewhat resemble the rubbed polymer layers used to align liquid crystals (LC). From previous studies of the alignment of LC on various structured surfaces, two contradictory mechanisms were proposed: (i) a true epitaxy, i.e., the orientation is achieved via short-range intermolecular interactions at the overlayer−substrate interface, and (ii) a grapho-epitaxy (long-range elastic interactions), where the orientation is induced by a cooperative organization of the molecules which align along the ridges or surface defects.[9,10] In addition, the preferential nucleation of organic crystals on topographical defects located on organic single-crystal cleavage planes but with epitaxial relationships was also reported.[11,12]

In this paper, we report the study of the selective nucleation of 2-methyl-4-nitroaniline (MNA) crystals on nanostructured PTFE substrates. The MNA was chosen for its attractive specific second-order NLO properties.[13,14] In previous works, Levine et al.[13] have estimated some coefficients of the nonlinear susceptibility tensor (d_{11} and d_{12}) of crystalline MNA from the measurement of the SHG intensity of a single-crystal plate.

* To whom correspondence should be addressed. E-mail: Pascal.Damman@umh.ac.be.
[†] Université de Mons-Hainaut.
[‡] Ecole Normale Supérieure de Cachan.

(1) Wittmann, J. C.; Smith, P. *Nature* **1990**, *352*, 414.
(2) Hansma, H.; Motamedi, F.; Smith, P.; Hansma, P.; Wittmann, J. C. *Polymer* **1992**, *33*, 647.
(3) Dietz, P.; Hansma, P. K.; Ihn, K. J.; Motamedi, F.; Smith, P. *J. Mater. Sci.* **1993**, *28*, 1372.
(4) Damman, P.; Dosière, M.; Smith, P.; Wittmann, J. C. *J. Am. Chem. Soc.* **1995**, *117*, 1117.
(5) Damman, P.; Fougnies, C.; Dosière, M.; Wittmann, J. C. *Macromolecules* **1995**, *28*, 8272.
(6) Damman, P.; Dosière, M.; Brunel, M.; Wittmann, J. C. *J. Am. Chem. Soc.* **1997**, *119*, 4633.
(7) Damman, P.; Dosière, M.; Wittmann, J. C. *Macromolecules* **1997**, *30*, 8386.
(8) Damman, P.; Vallée, R.; Dosière, M.; Wittmann, J. C.; Toussaere, E.; Zyss, J. *Opt. Mater.* **1998**, *9*, 423.
(9) Feller, M. B.; Chen, W.; Shen, Y. R. *Phys. Rev. A* **1991**, *43*, 6778.
(10) Dennis, J. R.; Vogel, V. *J. Appl. Phys.* **1998**, *83*, 5195.
(11) Carter, P. W.; Ward, M. D. *J. Am. Chem. Soc.* **1993**, *115*, 11521.
(12) Bonafede, S.; Ward, M. D. *J. Am. Chem. Soc.* **1995**, *117*, 7853.
(13) Levine, B. F.; Bethea, C. G.; Thurmond, C. S.; Lynch, R. T.; Bernstein, J. L. *J. Appl. Phys.* **1979**, *50*, 2523.
(14) Lipscomb, G. F.; Garito, A. F.; Narang, R. S. *J. Chem. Phys.* **1981**, *75*, 1509.

10.1021/ja991894u CCC: $19.00
Published on Web 06/30/2000

However, the interpretation of the measured coefficients was made hazardous since the crystal structure of MNA was not yet solved. Later, Lipscomb et al.[14] have determined the crystal structure of MNA and measured some of the electrooptic coefficients.

The aim of the paper is to demonstrate that the combination of oriented crystal growth, grazing incidence X-ray diffraction (i.e., determination of the crystalline orientation), and second harmonic ellipsometry (i.e., measurement of the polarization dependence of the SHG intensity) gives a precise view of the NLO properties of such a crystalline material. In addition, the analysis of the crystallographic orientations and the evolution of the nucleation rate of MNA crystals will give us the opportunity to discuss the possible orientation mechanisms.

Experimental Section

Materials. MNA (T_m = 131 °C) was purchased from Janssen Chimica Company and used without further purification. The oriented PTFE substrates were prepared according to the method previously described,[1−8] by sliding at constant speed, pressure, and temperature a PTFE rod against glass sides or silicon wafers. The orientation and thickness of the PTFE thin films were previously investigated by transmission electron microscopy and AFM.[2,3] In fact, these substrates are made of ordered (100) crystallographic surfaces with regularly stacked polymer chains and of numerous topographical defects such as ridges and grooves.

The crystalline layers of MNA were directly prepared on the PTFE substrates either by sublimation under vacuum (∼0.05 Torr) or from solution in water, ethanol, or methanol. The degree of supersaturation of the crystal growth experiments was estimated from the following parameters: (i) for the sublimation experiments, the temperatures of the MNA vapor and the PTFE substrate, controlled by immersing the flat bottom of a Pyrex tube in an oil bath thermostat and by using a water-cooled finger, respectively (the vapors and substrate temperatures range from 40 to 120 °C and from 0 to 40 °C, respectively); and (ii) for the solution experiments, the temperature of the MNA solutions and the PTFE substrate (i.e., the supersaturation is achieved by a temperature jump instead of the evaporation of the solvent). In some cases, MNA layers were annealed at temperatures close to the melting temperature of MNA crystals.

Characterization of the Crystalline Layers. The polarized light microscopic observations were carried out with a Leica DMR microscope fitted with an Orthomat photographic system. Diffraction and Grazing Incidence X-ray diffraction (GIXD) measurements were performed with a X-ray beam generated by a rotating anode (Rigaku Denki, RU300 18kW). A monochromatic X-ray beam was obtained with a plane graphite single crystal giving the K_α line of Cu (λ = 0.1542 nm). The scattering measurements were made using a four-circle diffractometer, a line focus, and a NaI scintillation detector. Different experimental geometries were used to investigate the planar and azimuthal orientations of the crystalline layers. The planar orientation was determined from classical $\theta-2\theta$ scans, the lattice planes parallel to the substrate surface being investigated. The azimuthal orientation was deduced from grazing incidence measurements (GIXD). In fact, the GIXD geometry allows the determination of the lattice planes perpendicular to the substrate. In terms of the transfer momentum vector **q**, the $\theta-2\theta$ and the grazing incidence reflections correspond to **q** vectors perpendicular and parallel to the substrate plane, respectively. During the GIXD experiments, the X-ray beam and the detector deviate from the sample plane by an angle of 0.5°. This incidence angle was set slightly higher than the critical angle (about 0.2° for such an organic compound) to ensure that the complete overlayer participates to the diffraction intensity.[15−17] The φ angle determines the angular position of the sample with respect to the incident X-ray beam. The zero position in φ corresponds to the PTFE chain axis perpendicular to the beam.

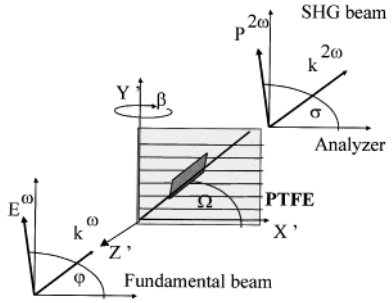

Figure 1. Sketch of the NLO second harmonic experiments (q, p, and s refer to orientation of the polarizers and/or analyzers). In the Maker's fringe and ellipsometry experiments the incidence angle (β) and the polarization angle (φ) vary from −60° to 60° and from 0° to 360°, respectively.

The NLO properties of the MNA crystalline layers were determined from second harmonic ellipsometry experiments. A Nd:YAG laser operating in Q switch mode, generating 30 ns pulses at a 10 Hz repetition rate, was used. The wavelength was set at 1340 nm to ensure that the generated second harmonic at 670 nm was not absorbed by the MNA crystals, the maximum of absorption in the visible spectra being close to 450 nm. The samples were mounted on a rotation stage, the PTFE chain axis (sliding direction) being perpendicular to the β rotation axis which defines the incidence angle of the laser beam (Figure 1). For such oriented layers, the polarization directions of the polarizer and analyzer have to be defined with respect to the substrate. The letters p and s refer to the polarization direction parallel and perpendicular to the PTFE axis, respectively. Absolute SHG intensity was determined from canonical Maker's fringes experiments in the so-called p−p polarization setup; a Y-cut single crystalline quartz slab was used as reference. Second, the polarization dependence of the SH signal was recorded with a nonlinear ellipsometry configuration. The intensity of the 2ω beam was measured under a normal incidence with both the q−p and q−s polarization setup (q indicates a 0−360° variable polarization angle).

Results and Discussion

Let us first recall some previous results about the crystal structure of MNA. The crystals adopt a I_a monoclinic structure (i.e., a non-standard setting of the C_c space group C_s^4)[18] with a = 0.823 nm, b = 1.162 nm, c = 0.759 nm, and β = 94.1°.[14] No evidence of polymorphism was reported up to now. This monoclinic I_a unit cell contains four symmetry related molecules, their dipole moments being nearly aligned.[14] The crystal has therefore a highly acentric polar structure. The dipole moments of individual molecules are tilted with respect to the (010) plane, one molecule pointing up coupled with another pointing down. These two molecules are obviously related by the glide plane of symmetry parallel to the a axis. Because of this symmetry element, the component of the dipole moment perpendicular to the (010) plane vanishes. The two other molecules in the unit cell are obtained by the centering of the cell, i.e., there are two lattice points per unit cell. The polar axis, given by the direction of the total dipole moment of the unit cell, lies in the (010) plane and is parallel to the [201] axis of the crystal.

Nucleation and Growth of MNA Crystalline Layers on PTFE Substrates. As shown in Figure 2, MNA deposited on PTFE substrates forms uniformly oriented layers made of numerous single crystals. To investigate the ability of the substrates to induce the crystal growth, the nucleation density of MNA crystals grown from vapor phase (i.e., the number of

(15) Brunel, M.; de Bergevin, F. *Acta Crystallogr.* **1986**, *A42*, 299.
(16) Feidenhans'l, R. *Surf. Sci. Rep.* **1989**, *10*, 105.
(17) Fuoss, P.; Eisenberger, P. *Synchrotron Radiation Research Advances in Surface Science*; Bachrach, R. Z., Ed.; Plenum: New York, 1991.
(18) Hahn, T. *International Tables of Crystallography*; Kluwer: Dordrecht, 1995; Vol. III.

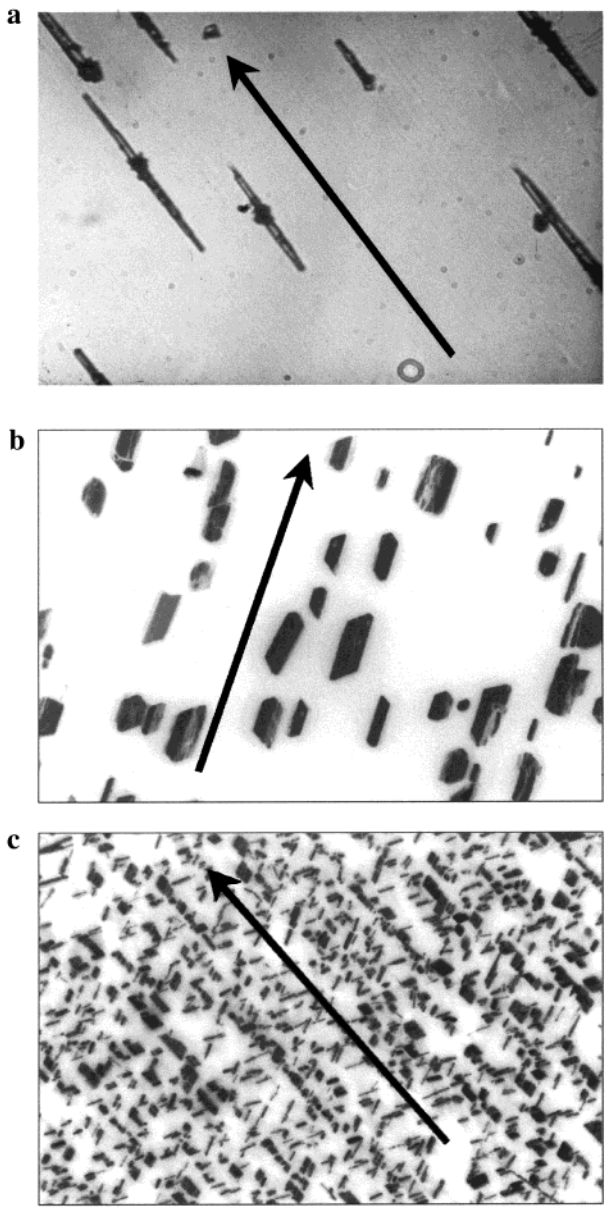

Figure 2. Optical micrographs of the MNA crystalline layers grown on PTFE substrates from the vapor phase (substrate temperature equal to 10 °C (a) and 40 °C (b)) and from supersaturated aqueous solution (c). The arrows indicate the PTFE sliding direction (i.e., the polymer chain axis).

nucleation events per time and surface unit) was estimated for various vapor and substrate temperatures. As shown in Figure 3, the curves giving the nucleation density against the substrate temperature exhibit a drastic decrease of the nucleation density for temperatures close to and above 20 °C whatever the temperature of the vapor. In addition, these two growth modes, as deduced from the nucleation density analysis, are associated to distinct crystal morphologies. The MNA crystals grown on the PTFE substrate held at temperatures below 20 °C exhibit a well-defined sharp needle shape (Figure 2a) while a parallelogram shape is observed when the PTFE substrates are kept at temperatures above 20 °C (Figure 2b). However, it should be noted that, despite the occurrence of two different growth modes, the optical observations clearly show the alignment of MNA crystals along the PTFE sliding direction (Figure 2). Annealing of the MNA layers was also used to improve the quality of the orientation and to increase the size of the MNA crystals grown by sublimation. The best results were obtained

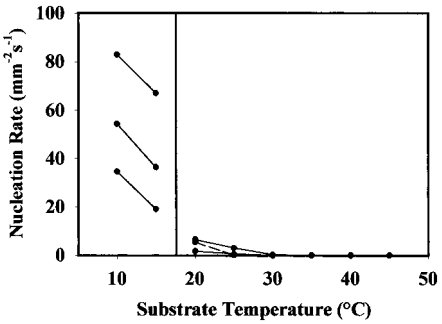

Figure 3. Plot of the nucleation rate of MNA crystals grown on oriented PTFE substrates from the vapor phase against the substrate temperature. The different curves refer to different vapor temperatures. The vertical line separates the low and high substrate temperature growth modes.

for annealing at temperatures close to the melting temperature of MNA crystals. It should be noted that the selection of a specific crystallographic contact plane (low or high temperature form) is determined during nucleation and maintained during annealing.

For the samples prepared from supersaturated solutions (wet process), the crystals also exhibit a unique orientation with respect to the PTFE substrate (Figure 2c). The crystal shape corresponds to parallelograms similar to those obtained from the vapor phase at high substrate temperature, the facets perpendicular to the substrate plane showing angles of 0° and 68.5° with the sliding direction of the PTFE films (chain axis).

These two different morphologies which unambiguously indicate the existence of two modes of crystal growth were then characterized by GIXD to determine the nature of the orientation and the relationships between the MNA and PTFE lattices.

Crystalline and Molecular Orientation of MNA on PTFE Substrates. (a) X-ray Diffraction. As shown in the Experimental Section, planar (i.e., the crystallographic plane in contact with the substrate) and azimuthal (i.e., the crystallographic axis parallel to the sliding direction) orientations of the crystalline thin layers can be deduced from $\theta-2\theta$ ($q_\perp$) and grazing incidence X-ray diffraction ($q_{//}$), respectively.

(i) Planar Orientation. The $\theta-2\theta$ diffraction curves recorded for various MNA layers grown on nanostructured PTFE are shown in Figure 4. For the low-temperature sublimated layer, the single observed reflection (Miller indexes (11−2), $\theta_{11-2} = 13.18°$, $q_\perp = 18.58$ nm^{-1}) indicates that the MNA crystals contact the (100) plane of PTFE with their (11−2) crystallographic planes. For the MNA crystals grown at temperatures above the order−disorder phase transition of PTFE ($T_{sub} = 40$ °C), the $\theta-2\theta$ diffraction curves exhibit two reflections (Miller indexes (11−2) and (020), $\theta_{020} = 7.62°$, $q_\perp = 10.81$ nm^{-1}), their relative intensity depending on the growth conditions. These observations clearly show that, for high-temperature growths, the PTFE substrate is covered by MNA crystals with either (11−2) or (010) crystallographic contact planes. In addition, as evidenced by the intense (020) reflection observed in the $\theta-2\theta$ diffraction curve, the MNA crystals grown on PTFE from supersaturated solutions (wet process) contact the substrate with their (010) crystallographic planes. Finally, the investigations of annealed layers clearly show that the initial orientation is maintained whatever the temperature and time of annealing. For instance, the diffraction curves, recorded for a layer sublimated at low temperature and further annealed at ∼130 °C during increasing times, only exhibit the (11−2) reflection characteristic of the (11−2) contact plane. However, for the MNA layers sublimated at high temperatures which are usually

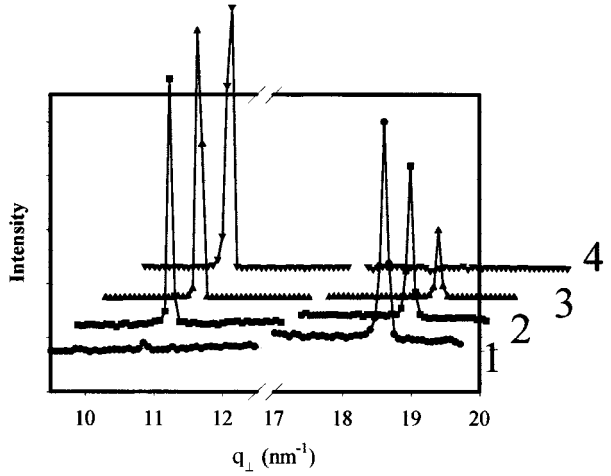

Figure 4. X-ray diffraction curves recorded with a $\theta-2\theta$ geometry (i.e., crystallographic planes parallel to the substrate, momentum transfer $q_\perp$) for MNA crystalline layers grown on PTFE substrates with various experimental conditions. The samples were prepared from vapors at $T_{sub} = 10$ °C (1), vapors at 35 °C (2), vapors at 35 °C and further annealed at 100 °C (3) and, finally, a supersaturated aqueous solution (4). The diffraction curves are shifted in intensity and q position for clarity.

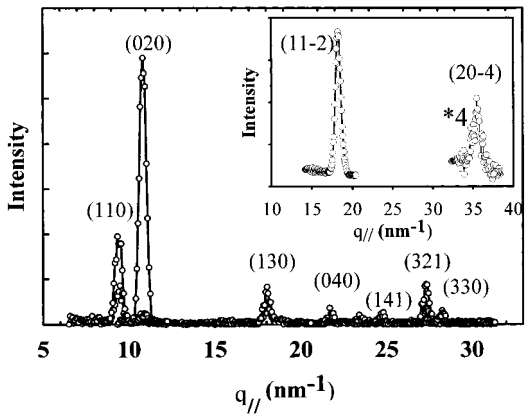

Figure 5. Grazing incidence X-ray diffraction curves (i.e., crystallographic planes perpendicular to the substrate, momentum transfer $q_{||}$) for a MNA layer grown on PTFE from the vapor phase at 10 °C. The inset shows the GIXD curves recorded for a MNA sample grown with a substrate temperature of 35 °C.

made of mixed (11−2) and (010) orientations, the annealing processes decrease the (11−2) low-temperature contribution, which completely vanishes for long annealing times.

(ii) Azimuthal Orientation. After the determination of the crystallographic plane in contact with the PTFE substrate, we focus on the azimuthal orientation that is defined by the orientation of the MNA lattice vectors with respect to the PTFE sliding direction. As shown here above, this can be achieved by using a grazing incidence diffraction geometry that allows the determination of the nature and orientation of crystal planes normal to the substrate surface ($q_{||}$ transfer momentum vectors).

First of all, the orientation of the indicatrix observed by polarized optical microscopy strongly suggests that the crystal polar axes are aligned along the PTFE sliding direction. Figure 5 shows selected GIXD curves recorded for MNA layers grown on PTFE at different substrate temperatures ($T_{sub} = 10$, 35 °C). The maxima observed in the intensity curves recorded with a variable φ angle, e.g., for the (020) reflection, obviously confirm the single crystal like orientation of the layer, a constant intensity being expected for isotropic or homeotropic layers. The Miller indexes of the observed diffraction peaks, together with their angular position (φ) with respect to the PTFE chain axis direction, are reported in Table 1. All the observed reflections were indexed with the previously reported monoclinic I_a unit cell. For the layers grown at low substrate temperatures, the examination of Table 1 shows that the $q_{||}$ vector related to the (020) reflection is normal to the PTFE sliding direction. From the Miller indexes of the contact plane and this observation, we can conclude that the polar axes of the MNA crystals (parallel to the [201] zone axis) are oriented along the PTFE chain axis, i.e., parallel to the [001] zone axis of PTFE. The crystallographic lattice relationships for the low-temperature growth of the MNA crystals on PTFE can then be summarized as follows:

Table 1. Grazing Incidence X-ray Diffraction Data[a]

(*hkl*)	θ (deg)	$q_{||}$ (nm^{-1})	φ_{obs} (deg)	φ_{calc} (deg)
low substrate temperature, (11−2) contact plane				
(110)	6.6	9.37	40.0	37.2
(020)	7.6	10.78	90.1	90.0
(130)	12.7	17.92	66.6	66.3
(040)	15.4	21.64	89.5	90.0
(141)	17.6	24.64	64.0	63.7
(321)	19.5	27.21	23.2	23.4
(330)	20.2	28.14	40.7	37.2
high substrate temperature, (010) contact plane				
(11−2)	13.2	18.61	89.4	90.0
(20−4)	25.9	35.60	90.1	90.0

[a] θ, $q_{||}$, φ_{obs}, and φ_{calc} refer to the diffraction angle, the transfer momentum, and the azimuthal position (observed and calculated) of the reflection with respect to the PTFE sliding direction, respectively

$$(1\ 1\ -2)_{MNA}||(1\ 0\ 0)_{PTFE}$$

$$[2\ 0\ 1]_{MNA}||[0\ 0\ 1]_{PTFE}$$

where ( ) and [ ] refer to lattice planes and zone axes, respectively. For the MNA layers grown at "high substrate temperature", two reflections are observed in the GIXD curves (see the inset of Figure 5). The azimuthal orientation observed for these reflections (see the φ_{obs} angles in Table 1) clearly shows that, as for the "low substrate temperature" growth, the crystal polar axis (i.e., the [201] zone axis) is parallel to the PTFE sliding direction. As indicated by the (20−4) reflection (see Table 1), the major difference with the previously described (11−2) "low substrate temperature" orientation arises from the lattice periodicity perpendicular to the PTFE chain axis. The orientation relationships therefore become:

$$(0\ 1\ 0)_{MNA}||(1\ 0\ 0)_{PTFE}$$

$$[2\ 0\ 1]_{MNA}||[0\ 0\ 1]_{PTFE}$$

(b) Overlayer−Substrate Interfaces. Depending on the substrate temperature, the MNA crystals grow on PTFE substrates with two different modes of crystallization related to the (11−2) or (010) orientations. As shown by the evolution of the nucleation rate (Figure 3), the transition between these modes of crystallization occurs around 20 °C and is accompanied by a sharp decrease of the nucleation rate when the substrate temperature becomes higher than 20 °C. These observations can be rationalized by considering the first order−disorder phase transition of PTFE. For clarity, we use the following notation to describe the 2D cells at the interface: b1, b2, β for the MNA overlayer and a1, a2, α for the PTFE substrate.

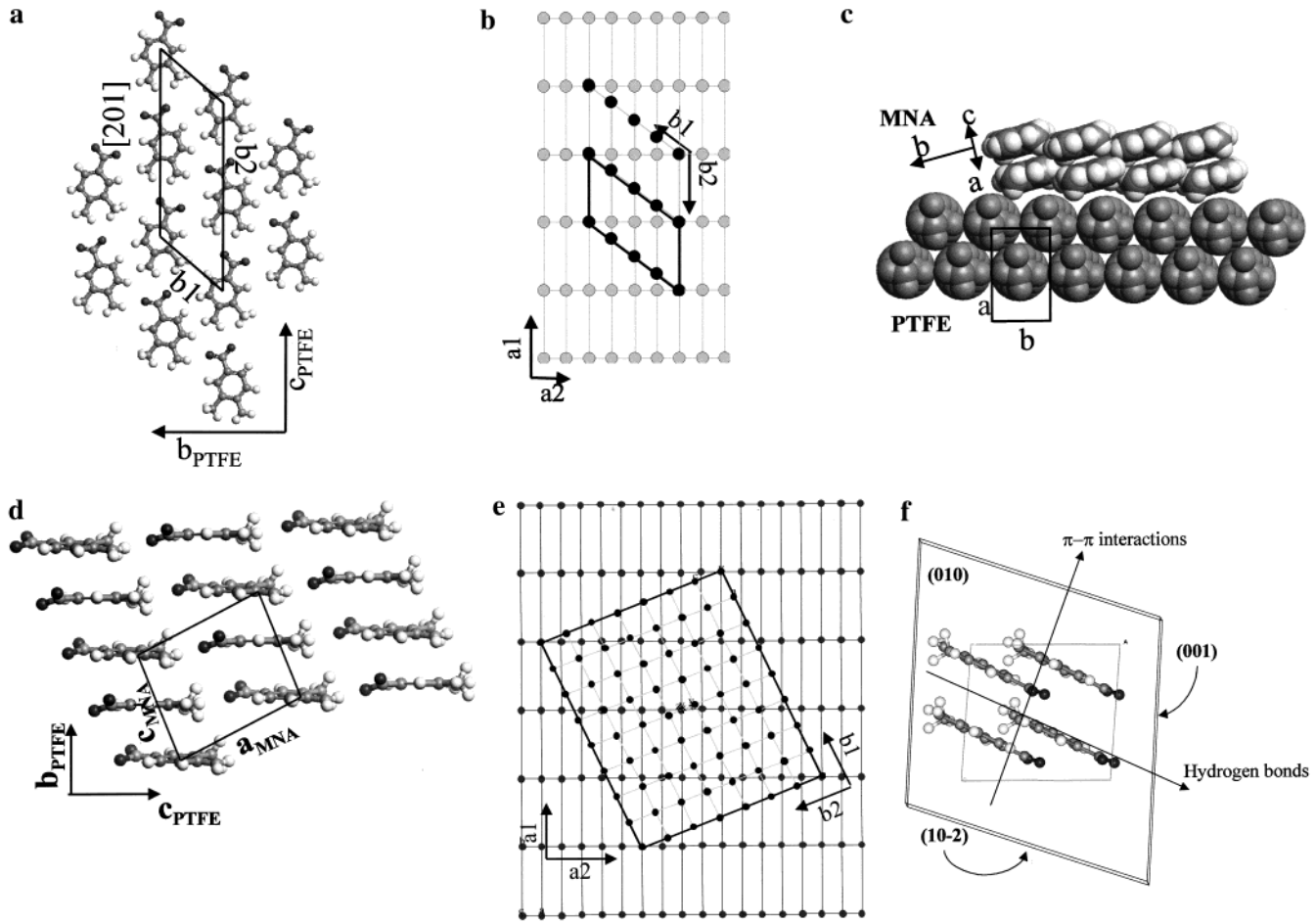

Figure 6. Molecular models of the MNA crystal structure and molecular packing in the different crystallographic planes in contact with the PTFE substrate: (a) (11−2) crystallographic plane of the MNA and lattice relationships with the PTFE substrate; (b) schematic description of the coincident overlayer with b1 = 0.79 nm, b2 = 1.76 nm ($[201]_{MNA}$), and $\beta = 50.0°$ (a1 = 0.56 nm, a2 = 1.70 nm, and $\alpha = 90°$). The 4 × 1 non-primitive supercell, commensurate with the substrate, is indicated (thick lines); (c) molecular model of the $(11-2)_{MNA}-(100)_{PTFE}$ interface; (d) model of the (010) crystallographic plane (molecules edge-on); (e) schematic description of the coincident overlayer with b1 = 0.823 nm, b2 = 0.759 nm, and $\beta = 94.1°$ (a1 = 0.566 nm, a2 = 1.95 nm, and $\alpha = 90°$). The 8 × 7 non-primitive supercell, commensurate with the substrate, is also indicated (thick lines); and (f) relation between the crystal shape and the intermolecular interactions in the unit cell.

Below 19 °C, the PTFE crystals are formed by the regular packing of 13_6 helices. An orthorhombic unit cell, with $a = 0.968$ nm, $b = 0.559$ nm, and $c = 1.69$ nm as parameters, containing two alternately right and left helices was proposed.[19−21] Although no commensurism is found, the low-temperature (11−2) MNA overlayer is characterized by a coincidence epitaxy with the (100) plane of the PTFE substrate, in agreement with the preferred azimuthal orientation.[22,23] The (11−2) MNA and (100) PTFE crystallographic planes correspond to 2D rectangular cells with b1 = 0.79 nm, b2 = 1.76 nm ($[201]_{MNA}$), and $\beta = 50.0°$ (Figure 6a) and a1 = 0.56 nm ($[010]_{PTFE}$), a2 = 1.70 nm ($[001]_{PTFE}$), and $\alpha = 90°$. According to Figure 6b and the orientation deduced from the X-ray investigations, the coincidence epitaxy is achieved at the overlayer−substrate interface for a 4 b1 × b2 oblique supercell (area: 4.26 nm^2) that becomes commensurate with the substrate. Considering the cell dimensions, directly computed from bulk crystal structures, the mismatches between overlayer and substrate lattices are rather small (the average Δ is equal to 6%). Figure 6c illustrates the molecular docking of the (11−2) crystal plane of MNA on the (100) PTFE surface and shows that MNA molecules are in the proper orientation to be in close interaction with the PTFE 13_6 helices.

Above the order−disorder phase transition at 19 °C, the PTFE crystals spontaneously transform into a "plastic crystalline" phase characterized by a change of the helical conformation (15_7 helix) and a lack of long-range orientational order along the PTFE chain axis. Previous experimental studies have shown a drastic increase in the number of chain defects such as reversal of the helical hand along the chain.[24,25] Due to the statistic average of the chain orientation, the unit cell becomes hexagonal with $a = b = 0.566$ nm, $c = 1.95$ nm, $\gamma = 120°$.[26] According to the GIXD results, the overlayer−substrate interface is made from the $(010)_{MNA}$ and $(100)_{PTFE}$ crystal planes. From the bulk crystal structure, these 2D lattices can be described by a 2D oblique cell (b1 = 0.823 nm ($[100]_{MNA}$), b2 = 0.759 nm ($[001]_{MNA}$), and $\beta = 94.1°$ see Figure 6d) and a 2D rectangular cell (a1 = 0.566 nm ($[010]_{PTFE}$), a2 = 1.95 nm ($[001]_{PTFE}$),

(19) Clark, E. S.; Muus, L. T. *Z. Kristallogr.* **1962**, *117*, 119.
(20) Weeks, J. J.; Clark, E. S.; Eby, R. K. *Polymer* **1981**, *22*, 1480.
(21) Clark, E. S. *J. Macromol. Sci. Phys. Ed.* **1967**, B1, 795.
(22) Hillier, A. C.; Ward, M. D. *Phys. Rev. B* **1996**, *54*, 14037.
(23) Last, J. A.; Hillier, A. C.; Hooks, D. E.; Maxson, J. B.; Ward, M. D. *Chem. Mater.* **1998**, *10*, 422.
(24) Corradini, P.; Guerra, G. *Macromolecules* **1977**, *10*, 1410.
(25) Kimmig, M.; Strobl, G.; Stuhn, B. *Macromolecules* **1994**, *27*, 2481.
(26) Bunn, C. W.; Howells, E. R. *Nature* **1954**, *174*, 549.

and $\alpha = 90°$) for $(010)_{MNA}$ and $(100)_{PTFE}$ planes, respectively. As for the low-temperature deposit, a coincidence epitaxy can be achieved for these lattices with the proper orientation determined by GIXD. Indeed, the 8 b1 × 7 b2 non-primitive supercell (area: 34.89 nm^2) is commensurate with the substrate (Figure 6e). However, the size of that supercell is about 10 times larger than the one observed for the (11−2) orientation.

(c) Nucleation of MNA Crystals: Orientation Mechanisms. The two modes of crystal growth observed for MNA on PTFE can be qualitatively described by considering the nucleation process. The heterogeneous nucleation of crystals on a substrate is mainly determined by the mother phase−crystal interfaces, the overlayer−substrate interface, and the bulk free energy of crystallization.[27] The free energy of a nucleus growing on a substrate can be written as the following

$$\Delta G_{nuc} = \sum_{hkl} A_{hkl} \cdot \gamma_{hkl} - A_{os} \cdot \gamma_{os} - \Delta G_c$$

where A, γ, and ΔG_c are the area and the surface free energy of the crystal facet, and the free energy associated with the phase change. The *hkl* and os subscripts refer to the (*hkl*) growing facet and the overlayer−substrate, respectively.

A key feature to describe the nucleation process of a crystal is to determine its shape. According to the Hartmann−Perdok theory, the shape of a crystal grown from the vapor phase can be related to the molecular packing and the strength of the intermolecular forces between molecules in the unit cell.[28,29] Indeed, the external shape of a crystal is determined by the growth rates which are roughly proportional to the attachment energy of the molecules to the crystal faces. For MNA, the strongest interactions are the $\pi-\pi$ interactions between superimposed aromatic rings and the hydrogen bonding along the polar axis (Figure 6f). These considerations are in agreement with the thin platelet single crystals previously observed for MNA.[13,14] The smallest faces (i.e., the fastest growing facets), indexed as (001) and (10−2), are related to the direction of the $\pi-\pi$ interactions and hydrogen bonding.

At low temperature, the MNA crystals contact the substrate with their small (11−2) facets (tilted by 16° with respect to the (10−2) face). By considering that the shape of MNA crystals corresponds to thin lamellae, these crystals are growing on the substrate with almost an edge-on orientation, highly unfavorable in terms of surface creation (see the expression of ΔG_{nuc} here above). The predominance of the (11−2) orientation therefore indicates that specific interactions occur at the $(11-2)_{MNA}$−$(100)_{PTFE}$ interface. Indeed, as shown here above (overlayer−substrate interfaces), the ordered structure of the PTFE (100) plane observed at low temperatures, containing regularly packed left- or right-handed helices, is particularly suitable to promote the growth of the MNA crystals. In fact, the van der Waals intermolecular interactions at the interface very likely induce a physisorption of the MNA aromatic molecules in order to nucleate the (11−2) orientation (Figure 6c).

At high temperature, the observed (010) planar orientation can be explained by considering the strong anisotropy of the MNA platelet crystals which tend to flatten on the substrate to minimize the total free energy of nucleation (i.e., the minimization of the total area of created surfaces). The alignment of the crystal polar axis along the PTFE sliding direction (i.e., the azimuthal orientation) can be accounted for by considering the following: (i) the topography of the substrate at the interface (grapho-epitaxy) [in fact, for rodlike molecules such as MNA, the bulk elastic energy is minimized when the long axis of the molecules is parallel to ridges and grooves of the PTFE surface[30]], and (ii) the formation of intermolecular interactions, between aromatic rings and the polymer chains, described by the supercell defined here above (Figure 6e). However, we should note that, in agreement with the drastic decrease observed for the crystal nucleation rate, the very large size of the super cell (34.89 nm^2) indicates that the interaction between the overlayer and the substrate planes is very poor. In fact, for such a large supercell the number of noncommensurate molecules is large and leads to an interfacial stress that makes this overlayer less energetically favorable than a smaller supercell.[22,23]

Quadratic Nonlinear Optical Properties of Oriented MNA Layers. The NLO properties of the MNA layers were determined from second harmonic ellipsometry and Maker's fringes measurements. As shown here above, the thin layers consist of a large number of MNA single crystals, their size being smaller than the size of the fundamental laser beam (1 mm in diameter). The phases of the contributions of the different crystals are therefore not spatially correlated. The overall second harmonic intensity collected by the detector is then the sum of the second harmonic intensities emitted by each crystal and can then be expressed as an orientation average of the individual intensities according to the orientation distribution probability of the crystals $f(\Omega)$:

$$I(\theta,\varphi) = \int_\Omega f(\Omega)\delta I(\Omega,\sigma,\varphi)\, d\Omega \qquad (1)$$

where φ and σ define the polarization direction of the fundamental and the second harmonic beams relative to the PTFE sliding direction. The angle Ω is defined with respect to the PTFE sliding direction (Figure 1). The δI refers to the intensity of one MNA single crystal.

In the following, the orthogonal reference frame (PTFE substrate) is defined with the X′ axis parallel to the PTFE chain axis, Y′ being in the plane of the layer. The nonlinear tensor $\chi^{(2)}$ is defined with respect to the principal dielectric frame of the MNA single crystal (*X*, *Y*, *Z*). According to Levine et al.[13] and Lipscomb et al.,[14] the *Z* axis is parallel to the *b* crystallographic parameter, the *X* axis being aligned along the crystal polar axis. The φ and Ω angles are therefore azimuthal and polar angles relative to the (*XY*) plane or to the plane tilted by 16° from the (*XZ*) plane, for $(010)_{MNA}$ or $(11-2)_{MNA}$ orientations, respectively. The SHG efficiency of a crystal is directly related to its nonlinear polarization, if one neglects the difference between transmission coefficients due to the birefringence of the crystals. Calling E_ω the fundamental electric field amplitude, one gets for the induced nonlinear optical polarization of MNA layers:

$$P^{(2)}_{2\omega} = 2 \cdot [d] \cdot E_\omega E_\omega \qquad (2)$$

where [*d*] is the first nonlinear susceptibility tensor. In the experiments, the SHG signal was analyzed for an orientation either parallel (p configuration) or perpendicular (s configuration) to the PTFE chain axis. This signal can then be expressed either as a function of the angle of incidence (β) of the incident laser beam (Maker's fringes configuration) or as a function of the input polarization orientation given by the angle φ (second harmonic ellipsometry configuration).

(27) Tiller, W. A. *The Science of Crystallization, Microscopic Interfacial Phenomena*; Cambridge University Press: Cambridge, 1991.
(28) Liu, X. Y.; Bennema, P. *Phys. Rev. B* **1994**, *49*, 765.
(29) Liu, X. Y.; Bennema, P. *J. Cryst. Growth* **1996**, *166*, 117.
(30) Berreman, D. W. *Phys. Rev. Lett.* **1972**, *28*, 1683.

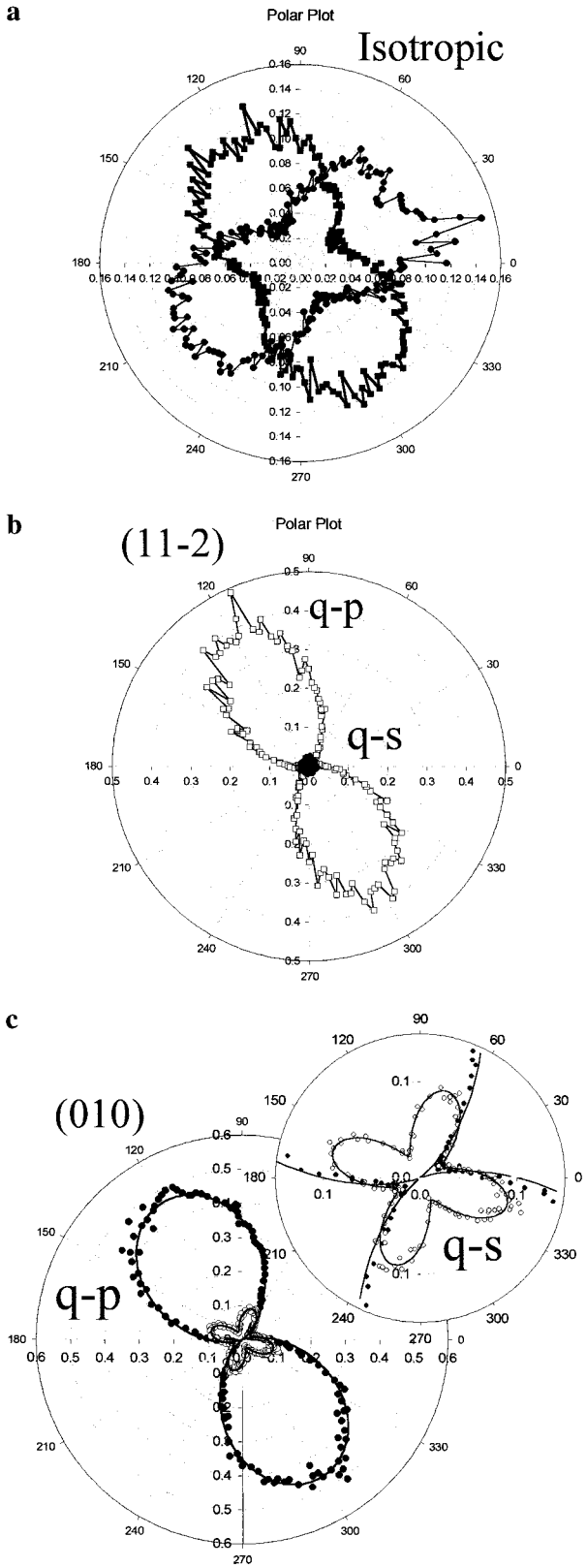

Figure 7. Polar plots of the polarization dependence of the second harmonic intensity (ellipsometry measurements) recorded in the q−p and q−s polarization setup as indicated. (a) Isotropic powder obtained by sublimation of MNA on bare glass, (b) (11−2) oriented layer grown on PTFE at a low substrate temperature (10 °C), and (c) (010) layer grown on PTFE at a high substrate temperature (35 °C).

(a) Second Harmonic Ellipsometry: Measurement. The polarization dependencies of the SHG signal for isotropic powder MNA samples and for the oriented samples grown on PTFE substrate were measured with the q−p and q−s experimental setup (Figure 7). In the isotropic case the two signals are obviously equivalent, since the characterization setup is invariant by any rotation around the optical beam axes (Figure 7a). For the oriented layers, two clearly different patterns were observed in Figure 7, parts b and c, for the (11−2) and (010) orientations, respectively. In both cases, a strong SH intensity is observed, in the q−p polarization, with two maxima over a complete rotation of the polarization direction (cos(2φ) dependence). In addition, for the (010) orientation a significant SH signal is also observed in the q−s polarization setup with four maxima over complete rotation (cos(4φ) dependence).

(b) Second Harmonic Ellipsometry: Analysis. For crystalline MNA in the monoclinic I_a space group (C_s symmetry, $m \perp Z$), the nonlinear polarization can be expressed with the d_{ij} components according to the relation[31]

$$\begin{pmatrix} P_x \\ P_y \\ P_z \end{pmatrix} = \begin{pmatrix} d_{11} & d_{12} & d_{13} & 0 & 0 & d_{16} \\ d_{21} & d_{22} & d_{23} & 0 & 0 & d_{26} \\ 0 & 0 & 0 & d_{34} & d_{35} & 0 \end{pmatrix} \cdot \begin{pmatrix} E_x^2 \\ E_y^2 \\ E_z^2 \\ 2E_yE_z \\ 2E_xE_z \\ 2E_xE_y \end{pmatrix} \quad (3)$$

By considering the Kleinman rules, the [d] tensor can be reduced with the following permutation symmetry:

$$\begin{Bmatrix} d_{11} = \chi_{XXX} \\ d_{22} = \chi_{YYY} \\ d_{12} = \chi_{XYY} = \chi_{YXY} = d_{26} \\ d_{13} = \chi_{XZZ} = \chi_{ZXZ} = d_{35} \\ d_{16} = \chi_{XXY} = \chi_{YXX} = d_{21} \\ d_{23} = \chi_{YZZz} = \chi_{ZYZ} = d_{34} \end{Bmatrix} \quad (4)$$

The XYZ frame corresponds to the dielectric frame defined here above. As a result of symmetry, the nonlinear tensor is reduced to six independent components. For the SHG measurements, the intensity at 2ω pulsation can be expressed as:

$$I_{2\omega} \propto |d_{\text{eff}}|^2 I_\omega^2 \quad (5)$$

where d_{eff} is the effective nonlinearity. In the second harmonic ellipsometry measurements, the polarization of the ω incident beam rotates in the plane of the substrate, the incidence angle being fixed at 0°. In this analysis, the angle φ is related to the direction of polarization with respect to the PTFE sliding direction. By considering the *XYZ* crystal frame, the wave vector of the fundamental beam is directed along the *Z* for the (010) orientation and tilted of 16° from *Y* for the (11−2) orientation.

For the (010) layers, the polarization direction scans the (*XY*) plane of the crystals. The expression of the effective nonlinear coefficient can then be expressed as the following

q−p polarization setup:

$$d_{\text{eff}} = d_{11} \cos^2 \varphi + 2d_{16} \cos \varphi \sin \varphi + d_{12} \sin^2 \varphi \quad (6)$$

q−s polarization setup:

$$d_{\text{eff}} = d_{16} \cos^2 \varphi + 2d_{12} \cos \varphi \sin \varphi + d_{22} \sin^2 \varphi \quad (7)$$

On the contrary, the polarization direction for the (11−2) layers is tilted by an angle ψ (i.e., the angle between (10−2) and (11−

2), equal to 16°) with respect to the *XZ* plane. The effective nonlinearity therefore becomes:

q−p polarization setup:

$$d_{\text{eff}} = d_{11}\cos^2\varphi + (d_{13} + (d_{12} - d_{13})\sin^2\psi)\sin^2\varphi - 2d_{21}\sin\varphi\cos\varphi\sin\psi \quad (8)$$

q−s polarization setup:

$$d_{\text{eff}} = -d_{21}\cos^2\varphi\sin\psi + [-d_{23}\sin\psi - 2d_{23}\sin\psi\cos^2\psi]\sin^2\varphi + 2(d_{12}\sin^2\psi + d_{13}\cos^2\psi)\cos\varphi\sin\varphi \quad (9)$$

These equations were used to analyze the experimental second harmonic ellipsometry curves recorded with a variable polarization (φ scan). First of all, the relative intensity measured for the (11−2) oriented layers with a q−p and q−s polarization setup shows that the d_{13} and d_{21} coefficients of the tensor are negligible with respect to the d_{11} coefficient (see eqs 8 and 9). In addition, the values of the fitting parameters obtained for the (010) oriented layer give us the opportunity to compute the ratio between the nonvanishing coefficients of the [*d*] tensor, d_{11} and d_{12}. The tensor components deduced from the SHG experiments can therefore be expressed as

$$\frac{d_{11}}{d_{12}} \approx 4 \quad (d_{13}, d_{21}, d_{22}, d_{16} \ll d_{11}, d_{12}) \quad (10)$$

We should note that our measurements are consistent with the study of a MNA single crystal reported by Levine et al., the measured ratio of d_{11}/d_{12} being equal to 6.[13]

(c) Maker's Fringes Experiments. In the limit case of the thin film, the maximum second harmonic intensity is proportional to the square of the nonlinear effective coefficient multiplied by the thickness (*L*):

$$I(2\omega) \propto (d_{\text{eff}}L)^2 \quad (11)$$

where *L* refers to the average thickness of the layer. From the intensity signal, the product of the MNA nonlinear coefficient and the sample thickness can be estimated by the square root of the maximum SHG intensity ratio taking into account the value measured for a quartz slab as reference:

$$(d_{\text{eff}}\cdot L_{\text{eff}})^{\text{powder}}_{\text{MNA}} = (d_{11}\cdot L)_{\text{Q}}\sqrt{\frac{I_{\max}(\text{MNA})}{I_{\max}(\text{Q})}}\ (\mu\text{m}\cdot\text{pm/V}) \quad (12)$$

where L_{eff} represents the effective thickness of the MNA layers (see below). As expected, similar results were obtained for both (11−2) and (010) crystal orientations since the crystal polar axis remains parallel to the PTFE sliding direction for both orientations. The values range between 4.6 and 24 μm·pm/V depending on the sample thickness and crystal size. The highest values were obtained for annealed samples exhibiting the biggest crystals. Since the crystals constituting one layer are not spatially correlated, an effective sample thickness (L_{eff}) corresponding to a true uniform correlated layer can be computed taking into account the d_{11} measured by Levine (d_{11} = 250 pm/V, coherence length of 0.7 μm). In our case, the computed L_{eff} values range between 0.02 and 0.1 μm, these values being consistent with the observed thickness of the samples (0.05−1 μm).

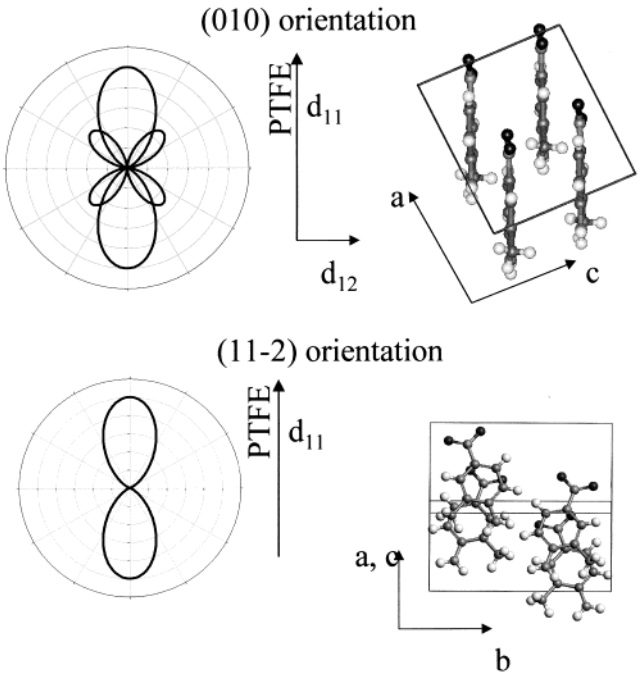

Figure 8. Schematic view of the relations between the second harmonic ellipsometry measurements and the crystallographic orientations (as indicated).

(d) Relation between Crystalline and Molecular Nonlinearity. As shown here above, the ability to prepare thin layers with two orthogonal crystalline orientations is very useful for studying the NLO properties of crystals. The results and the analysis of the polarization dependence of the SHG signal are summarized in Figure 8, together with the corresponding molecular orientation (we have considered the main coefficients d_{11} and d_{12}). The measurements of the nonlinear coefficients clearly show that $d_{11} > d_{12} \gg d_{13}$, ... for crystalline MNA. As we will see here below, these experimental values are in contradistinction with theoretical assumptions made within the currently accepted framework. In fact, the contributions to the nonlinear susceptibility tensor (χ) of organic crystals can be estimated from the molecular hyperpolarizability tensor (β). As previously proposed by several authors, for an aromatic planar molecule with C_s symmetry, the nonvanishing terms of the first hyperpolarizability are β_{xxx}, β_{xyy}, β_{yxx}, and β_{yyy}[32] (within the molecule frame, *x*, *y*, and *z* refer to the charge-transfer axis, the in-plane axis perpendicular to the charge-transfer direction, and the axis normal to the mirror plane). In the oriented gas model, the macroscopic susceptibilities $\chi^{(2)}$ related to the d_{ij} coefficients can be computed from the molecular hyperpolarizabilities according to the following relation

$$\chi_{IJK} = \sum_{s}\sum_{ijk}\cos\theta_{Ii}\cdot\cos\theta_{Jj}\cdot\cos\theta_{Kk}\cdot\beta_{ijk} \quad (13)$$

where *IJK*, *ijk*, and θ refer to the crystalline dielectric frame, the molecular frame and the projection angle of the molecular axes on dielectric axes, respectively. By considering the β_{ijk} defined here above and the orientation of the molecules in the unit cell,[14] the d_{11}, d_{12}, and d_{13} coefficients of the nonlinear

(31) Dmitriev, V. G.; Gurzadyan, G. G.; Nikogosyan, D. N. *Handbook of Nonlinear Optical Crystals*; Siegman, A. E., Ed.; Springer Series in Optical Science; Springer: New York, 1997.

(32) Chemla, D. S.; Zyss, J. *Nonlinear optical properties of organic molecules and crystals*; Academic Press: Orlando, 1987.

tensor were calculated from eq 13 and are expressed as

$$d_{11} = \chi_{XXX} = 2\cos^3 \alpha \cdot \beta_{xxx} + 2\cos \alpha \cdot \sin^2 \alpha \cdot \beta_{xyy}$$

$$d_{12} = \chi_{XYY} = 0$$

$$d_{13} = \chi_{XZZ} = 2\cos\alpha. \cdot \sin^2\alpha \cdot \beta_{xxx} + 2\cos^3\alpha \cdot \beta_{xyy} \quad (14)$$

where α is the angle between the molecular dipole moment and the *X* axis (direction of the crystal dipole moment). Therefore, in complete opposition to the experimental results, the values of the d_{ij} components of the susceptibility tensor computed for the MNA crystals show that $d_{11} > d_{13}$ and $d_{12} = 0$.

Why such a discrepancy? To account for the strong departure from the expected results, we suggest that either additional coefficients of the β tensor have to be considered (i.e., out of plane components such as β_{xzz}) or, more probably, the strong intermolecular interactions inside the crystal add unexpected coefficients in the *d* tensor. We should note that the additional d_{12} component observed for MNA corresponds to the direction of the strong $\pi-\pi$ intermolecular interactions between stacked aromatic molecules (Figure 8).

Conclusions

The study of the oriented growth of MNA crystals on highly oriented PTFE films prepared by the friction-transfer method has revealed specific features of these substrates. In fact, two single-crystal-like orientations with different nucleation rates were observed. The transition between these two modes of growth was related to the first order−disorder phase transition of the PTFE occurring at 19 °C. At "low substrate temperature", the ordered (100) PTFE surface induces the growth of MNA crystals, with a (11−2) coincidence epitaxy involving rather small supercell area and lattice mismatches, while at "high substrate temperature" the organic crystals are assumed to preferentially nucleate on topographical defects of the surface via a grapho-epitaxy mechanism.

This study also demonstrates the ability of oriented crystal growth combined to second harmonic ellipsometry to measure the components d_{ij} of the first optical nonlinear susceptibility tensor. Finally, the strong disagreement between the measured ratios between the d_{11}, d_{12}, d_{13}, ... coefficients and the theoretical estimation clearly shows that either the oriented gas model or the nonvanishing components of the hyperpolarizability tensor have to be questioned at least in the case of crystalline MNA.

Finally, it should be stressed that, despite the observed uniform orientation, the layers grown on the PTFE substrates are polycrystalline and that we were not able to produce large MNA single crystals with macroscopic size up to now.

Acknowledgment. This work was supported by the French Community of Belgium (CGRI-CNRS, "Tournesol" program 98.078), the CNRS, and the Belgian National Funds for Scientific Research (FNRS). P. Damman is a Research Associate of the FNRS.

JA991894U